

## Discharge state transition and cathode fall thickness evolution during chromium HiPIMS discharge

Xiao Zuo, Peiling Ke, Rende Chen, Xiaowei Li, Magnus Odén, and Aiying Wang

Citation: *Physics of Plasmas* **24**, 083507 (2017); doi: 10.1063/1.4995482

View online: <http://dx.doi.org/10.1063/1.4995482>

View Table of Contents: <http://aip.scitation.org/toc/php/24/8>

Published by the *American Institute of Physics*

---

---

**COMPLETELY  
REDESIGNED!**



**PHYSICS  
TODAY**

*Physics Today* Buyer's Guide  
Search with a purpose.

# Discharge state transition and cathode fall thickness evolution during chromium HiPIMS discharge

Xiao Zuo,<sup>1,2</sup> Peiling Ke,<sup>1,2</sup> Rende Chen,<sup>1,2</sup> Xiaowei Li,<sup>1,2</sup> Magnus Odén,<sup>3</sup> and Aiyang Wang<sup>1,2,a)</sup>

<sup>1</sup>Key Laboratory of Marine Materials and Related Technologies, Ningbo Institute of Materials Technology and Engineering, Chinese Academy of Sciences, Ningbo 315201, China

<sup>2</sup>Zhejiang Key Laboratory of Marine Materials and Protective Technologies, Ningbo Institute of Materials Technology and Engineering, Chinese Academy of Sciences, Ningbo 315201, China

<sup>3</sup>Department of Physics, Chemistry, and Biology, Linköping University, Linköping 58183, Sweden

(Received 16 May 2017; accepted 11 July 2017; published online 24 July 2017)

The temporal evolutions of target voltage and current waveforms under different pulse voltage and working pressure conditions were studied during Cr high power impulse magnetron sputtering discharges. Target voltage and current characteristics demonstrated that when the pulse width was set as 200  $\mu$ s, HiPIMS discharge went through a four-stage sequence during each pulse, Townsend discharge, glow discharge, afterglow, and pulse-off stages. A discharge state transition in the glow discharge stage happened at high pulse voltage and working pressure conditions. Furthermore, the dependence of reduced cathode fall thickness  $pd_c$  on pulse voltage, working pressure, and normalized current density  $j/p^2$  was presented. It was found that gas rarefaction leads to a change of relationship between  $pd_c$  and  $j/p^2$ . A noticeable increase of the cathode fall thickness caused by gas rarefaction has been found. *Published by AIP Publishing.* [<http://dx.doi.org/10.1063/1.4995482>]

## I. INTRODUCTION

Through applying a high power pulse on the target with a short pulse length and low duty cycle, high power impulse magnetron sputtering (HiPIMS) offers means to achieve high density plasma.<sup>1</sup> The result is a higher ionization rate of the sputtered material compared with direct current magnetron sputtering (DCMS).<sup>2</sup> The increased ionization rate favors the sputtering rate, suppresses target poisoning, and enhances the chemical activity of the precursors by the bombardment of energetic particles, which promotes substrate adhesion, film density, and surface smoothness.<sup>3</sup> These positive features make HiPIMS an attractive deposition technique for a range of applications including solar cells,<sup>4,5</sup> optoelectronic devices,<sup>6</sup> magnetoelectric materials,<sup>7</sup> surface protection coatings,<sup>8</sup> etc. However, a main disadvantage is the low deposition rate. HiPIMS deposition rates are typically 25%–35% of DCMS deposition rates at the same average discharge power for metals, oxides, and nitrides. The phenomenological model developed by Christie and Vlček suggested that the loss of the deposition rate is attributed to the high fraction of ionized sputtered atoms directed back to the target.<sup>9,10</sup> Moreover, plasma in the HiPIMS discharge is transient compared to the more stationary DCMS case, which makes its discharge more complex.<sup>1</sup> Factors such as pulse voltage waveform, magnetic field, gas precursors, working pressure, target material, etc. can all influence the HiPIMS discharge.<sup>11</sup> Understanding the plasma characteristics in a HiPIMS discharge is thus of great significance to solve the low film growth rate and to find process envelopes such that stable plasmas with high ionization can be sustained. A simple and practical method to characterize the discharge is to study target voltage and current

waveforms: Alami *et al.* investigated the voltage-current characteristics for different pulse voltages and identified the operation modes<sup>12</sup> and Anders *et al.* used current-voltage-time characteristics to describe the HiPIMS discharge and found a sustained self-sputtering process.<sup>13</sup> They concluded that HiPIMS discharges typically exhibited an initial pressure dependent current peak followed by a power and material dependent phase. The target current waveforms were related to target materials, and even more for the same target it showed distinct shapes at different pulse voltages and pressures.<sup>14</sup> Therefore, understanding the discharge states in HiPIMS operation modes under different working parameters would provide an instruction for controlling sputtering processes to satisfy specific application requirements. After more than 10 years of investigations, comprehensive understanding, reviewed by Gudmundsson *et al.*,<sup>1</sup> on several basic processes such as low deposition rate, neutral particle rarefaction, sputtered material ionization, and charged particle transportation in HiPIMS discharges was obtained. However, most of these research results were phenomenological and experimental experience. Nowadays, the unpreferred factors like low deposition rate, frequent arcing, and complex operation modes still limit the industrial application of HiPIMS for deposition of films or coatings. The literature concerned with discharge states behind each operation mode and the temporal evolution of the cathode fall thickness before and after gas rarefaction is still limited. The discharge state during each voltage pulse, the variation with working parameters, and the cathode fall thickness in the transient discharge need to be investigated.

Here, we discuss the measurements of target voltage and current waveforms during Cr HiPIMS discharge under different pulse voltage and working pressure conditions. The temporal evolution of the target voltage-current features in the transient discharge stage after the static breakdown of the

<sup>a)</sup>Electronic mail: aywang@nimte.ac.cn. Tel.: +86-574-86685170.

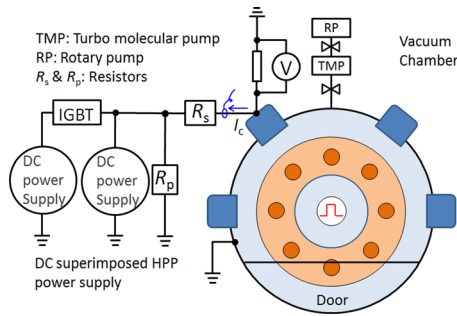


FIG. 1. Arrangement of the HiPIMS facilities and  $V_I$  measurement circuit.

working gas will be discussed. Four discharge stages were determined during each pulse. The normalized target current density  $j/p^2$  was obtained with a thin sheath model. Reduced cathode fall thickness  $pd_c$  was determined by the collisionless Child-Langmuir Law. The relationship between the reduced cathode fall thickness and the normalized current density was obtained. A noticeable increase of the reduced cathode fall thickness caused by gas rarefaction was found at high pulse voltage and high working pressure conditions. These results offer insights into the discharge states in different HiPIMS operation modes for targets with relatively high sputtering yield and second ionization energy.

## II. EXPERIMENTAL SETUP

HiPIMS discharge experiments were performed in a custom built cylindrical magnetron sputtering system,<sup>15</sup> 60 cm in diameter and 60 cm in height with a base pressure of

$1.5 \times 10^{-2}$  mTorr. The sputtering gas was argon (99.999% purity) and the gas flow rate was set to 50 sccm. The working pressure was adjusted precisely through a throttle valve and monitored continuously by a capacitance manometer. As a representative cathode material, a rectangular unbalanced planar magnetron source was fitted with a Cr target of 99.9% purity with the size of  $40 \text{ cm} \times 10 \text{ cm} \times 0.7 \text{ cm}$ . The magnetic field on the target surface was around 260 G. A high power pulse unit (HPPMS-20k, PTL) operating in unipolar mode was used to power the target. The target voltage and current were monitored using a combined current transducer (LEM LT58-S7) and voltage divider unit, as shown in Fig. 1. The data were recorded with a digital storage oscilloscope (Tektronix TDS 1012C-SC). The pulse length and repetition frequency were kept at  $200 \mu\text{s}$  and 50 Hz, respectively.

## III. RESULTS AND DISCUSSION

### A. The temporal evolution of target voltage and current

The voltage  $V_t$  measured at the target can be expressed by the following circuit equation:

$$V_t(t) = V_p - \frac{1}{C} \int I_t(t) dt - R \times I_t(t), \quad (1)$$

where  $V_p$  and  $I_t$  are pulse voltage and measured target current, respectively;  $C$  and  $R$  are the capacitance and resistance of the circuit. Figure 2 shows the influence of pulse voltage and working pressure on  $V_t$  and  $I_t$ . In the experiments, when pulse voltage was lower than 400 V, no discharge current

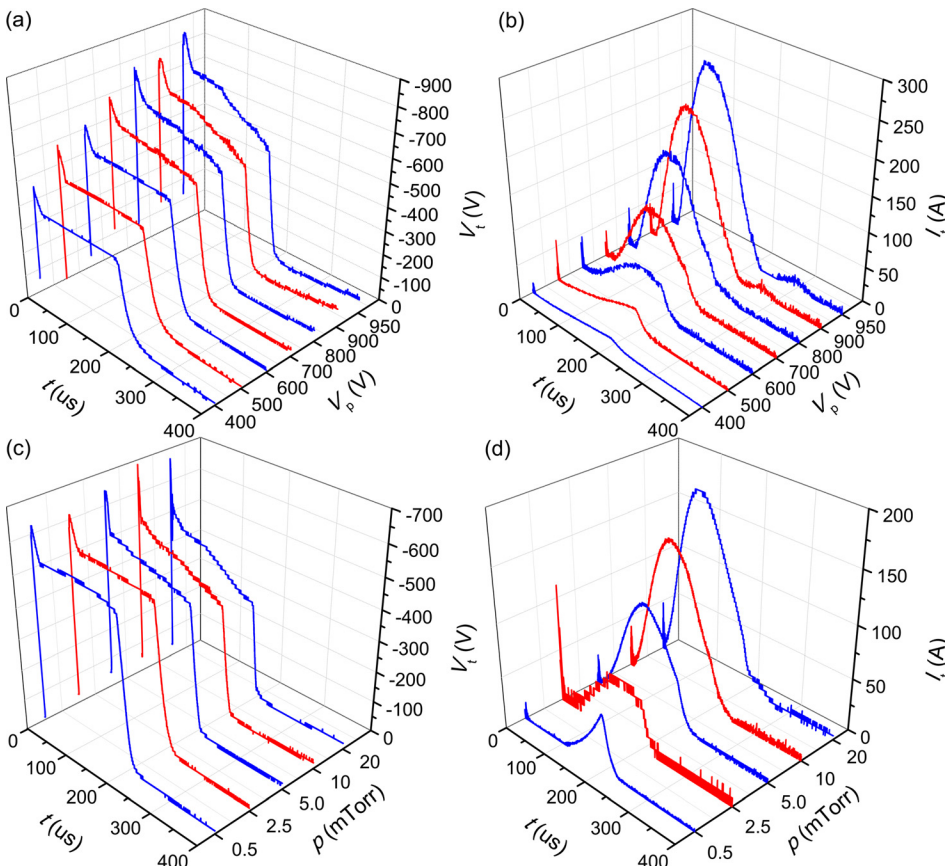


FIG. 2. Target voltage and current waveforms with the variation of pulse voltages and pressures. The pressure is 2.5 mTorr in (a) and (b), the pulse voltage is 600 V in (c) and (d).

signal was detected. HiPIMS discharge started to occur at pulse voltage around 400 V under the experimental conditions. After the gas breakdown, the target voltage decreased to 360 V and remained almost constant during the entire pulse. A pulse voltage of 500 V showed similar target voltage evolution to the 400 V case. However, above 600 V, the target voltage waveforms demonstrated a downward trend after breakdown. The target current spectra changed from triangular waveforms to hump-like waveforms [Fig. 2(b)] when the pulse voltage increased to 600 V, in particular under the higher pulse voltage condition. For target current evolution, highly oscillatory displacement current occurred before the gas breakdown and target current was detected immediately, and then it increased gradually with time to maximum after a delay to the voltage pulse. Meanwhile, increasing the pulse voltage resulted in the enhanced target current caused by high density plasma. As the working pressure increased, the temporal evolution of target voltage [Fig. 2(c)] and current [Fig. 2(d)] followed a similar trend to that observed under the various pulse voltage conditions, respectively. The decrease of target current was attributed to the gas rarefaction effect during the pulse stage.<sup>16</sup>

Figure 3 shows the target  $VI$  curves during a single pulse with representative pulse voltage at 500 and 700 V. It elucidates the discharge behaviors of the chromium HiPIMS process under a low or high pulse voltage, respectively. At high pulse voltage, as shown in Fig. 3(b), first, a sudden drop of voltage can be observed from  $A$  to  $B$ , then followed by a negative slope from  $B$  to  $C$ . These are typical characteristics for Townsend-to-glow discharge transition, and a transient glow

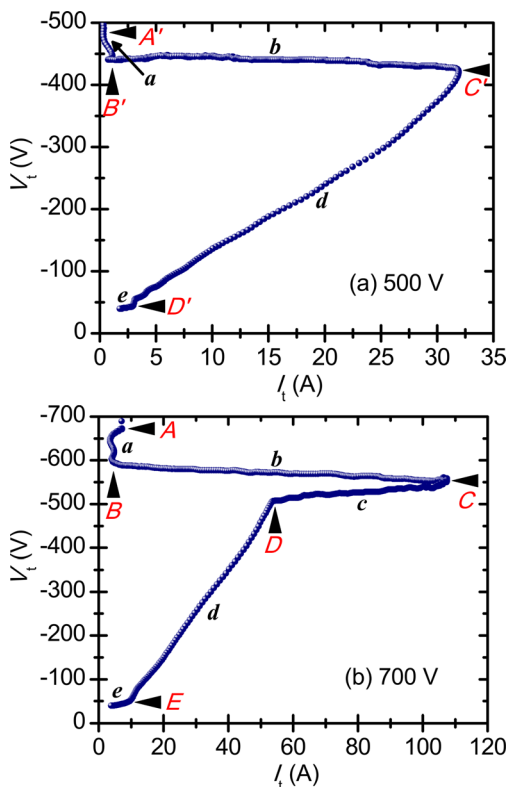


FIG. 3.  $VI$  curves of the Cr HiPIMS discharge with pulse voltage at 500 V (a) and 700 V (b).

discharge, respectively. The two positive slopes from  $C$  to  $D$  and from  $D$  to  $E$  correspond to abnormal glow ( $C-D$ ) and plasma afterglow ( $D-E$ ) in the electric circuit. However, at low pulse voltage HiPIMS discharge only experienced breakdown ( $A'-B'$ ), transient glow ( $B'-C'$ ), and plasma afterglow ( $C'-D'$ ) three stages. The decrease of both target voltage and current before plasma afterglow is not presented in Fig. 3(a). Similar processes can also be observed at low or high working pressure conditions.

Therefore, according to the  $VI$  characteristics and temporal evolution of  $V_t$  and  $I_t$ , a HiPIMS discharge pulse goes through four main stages: Townsend discharge and breakdown (stage  $a$ ), glow discharge (stage  $b$  &  $c$ ), afterglow (stage  $d$ ), and pulse-off (stage  $e$ ), as shown in Fig. 4. Stage  $a$  is the region between oscillatory displacement current and the increase of target current. The delay of current onset is mainly attributed to the time needed for electron magnetization and electron impact ionization.<sup>17</sup> At this stage, before breakdown, the system operates as a magnetized Townsend discharge. After breakdown, the target voltage decreases and the discharge is now in the glow discharge stage. At high pulse voltage or working pressure conditions, as a consequence of gas rarefaction caused by the instant high power, the target current starts to decrease after reaching maximum.<sup>16</sup> When the voltage pulse ends, the target voltage and current decrease with a time constant  $RC$  in the afterglow stage ( $d$ ). Finally, both target voltage and current become zero in the pulse-off stage ( $e$ ). It is noted that the current waveform is sinusoidal. This means that plasma density changes with time; in particular, the plasma density increases as the current increases. This causes unstable plasma, which could easily transit from the glow state to arc state. In order to maintain a stable HiPIMS plasma, the pulse width is suggested to be less than the time corresponding to the peak current. To obtain a constant plasma density, it is advised that the current waveform should be rectangular with a reduced current.

## B. Discharge state transition in the glow discharge stage

According to Eq. (1), the decrease of current usually results in an increase of target voltage. However, at high pulse voltage and working pressure conditions both of the target voltage and current suffered a decrease during stage  $c$ . This anomalous phenomenon could be attributed to a large amount of sputtered Cr atoms engaging in the discharge at

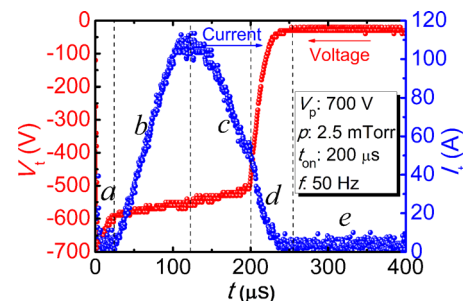


FIG. 4. Discharge stages in target voltage and current waveforms of the HiPIMS discharge.

high plasma density conditions. The lower ionization energy of Cr atoms than that of Ar would result in the decrease of breakdown voltage. To further understand the target voltage and current waveforms in terms of the relationship among glow discharge, pulse voltage, secondary electron emission yield, and cathode fall thickness,<sup>18</sup> we herein plot the target voltage  $V_t$  against normalized current density  $j/p^2$ , in where  $j$  is the current density over the plasma covered target surface and  $p$  is the working pressure. The shape of magnetron discharge is donut like. Under the HiPIMS discharge conditions, the energetic electron gyroradius is larger than the plasma sheath thickness as determined by the Child-Langmuir law. Therefore, electrons emitted from the target are accelerated through the plasma sheath, and then take the cyclotron motion back to the target surface. According to the thin sheath model,<sup>19,20</sup> the ionization region thickness is approximately the radius  $r_{ce}$  of the electron cyclotron circle at  $B_0$ . The width  $w$  of the ionization region can be calculated through the radius of curvature ( $R_c \approx 3$  cm) of the magnetic field line,<sup>20</sup>

$$w \approx 2(2r_{ce}R_c)^{1/2}, \quad r_{ce} = \frac{1}{B_0} \left( \frac{2mV_t}{e} \right)^{1/2}. \quad (2)$$

The current density  $j$  is assumed to be expressed as

$$j = I_t / 2(\pi R w + l w), \quad (3)$$

where  $R$  is the radius of the semi-circular racetrack and  $l$  is the length of the line racetrack.

Figure 5 shows the  $V_t$  versus  $j/p^2$  in the glow discharge stage (stage *b* & *c*) as a function of pulse voltage [Fig. 5(a)] and working pressure [Fig. 5(b)]. Two different regions corresponding to stage *b* and *c* in Fig. 4 are identified. The results

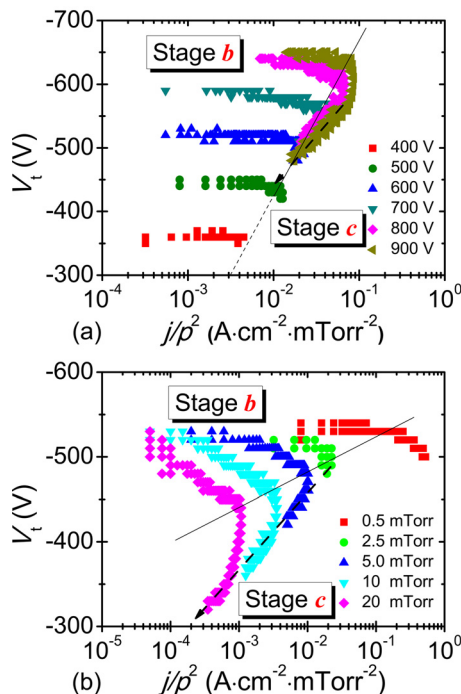


FIG. 5.  $V_t$  against  $j/p^2$  for stage *b* and *c* with different pulse voltages at 2.5 mTorr (a) and pressures at 600 V (b).

shown in Fig. 5(a) indicate that target voltage in stage *b* is determined by pulse voltage. With the increase of current density, target voltage decreases a little. However, in stage *c* there is a fast decrease in target voltage and reduction in current density when pulse voltage is higher than 600 V. This indicates typical abnormal glow in stage *c* at high pulse voltage conditions.<sup>21</sup> When the pulse voltage is lower than 600 V, the discharge state transition has not been detected. However, it becomes faster at higher pulse voltage and causes two different slopes in stage *c*. In the first segment, the target voltage drops to  $\sim 580$  V for pulse voltages higher than 700 V with  $j/p^2$  decreasing a little. In the second segment, it changes with a different slope independent of pulse voltage and all curves overlap. When the pulse voltage is high, high plasma density leads to an increased amount of sputtered material. This causes the voltage drop in the first segment. Meanwhile, gas rarefaction induced by heating is a time accumulative process. In the second segment, it becomes so severe that the sputtered material takes a great part in the discharge. Therefore, the two slopes in stage *c* reflected the transformation from the transient sputtering process to self-sputtering dominated process.

Similar to the results shown in Fig. 5(a), the evolution of the  $V_t$  with  $j/p^2$  in Fig. 5(b) can also be divided into two stages based on the curves' slope at different working pressures. In stage *b*, the target voltage is nearly independent of the current density in the case of a working pressure of 0.5 and 2.5 mTorr, which implies normal glow. However, further increasing the working pressure to a value between 2.5 and 20 mTorr, a significant decrease of target voltage is observed in stage *b*. Discharge in this stage is still under development. An even stronger drop of the target voltage combined with a reduction of current density is seen in stage *c*. For the various pulse voltage and working pressure conditions, the relationship between  $V_t$  and  $j/p^2$  is similar in the second segment of stage *c*.

Based on these features, it can be concluded that the discharge in stage *b* and *c* is a transient glow discharge. Once the pulse length is long enough, increasing pulse voltage and working pressure both cause gas rarefaction due to the ultra-high instant discharge power. Therefore, less gas precursors lead to the increase of the electron neutral mean free path, which reduces the probability of collision between electrons and Ar atoms. Hence, electrons can achieve higher kinetic energy to ionize more sputtered material, the sputtering process changes from gas sputtering to a self-sputtering dominated process. The drop in the target voltage and normalized current density indicates the approach to a steady state discharge.

### C. The evolution of the cathode fall thickness during glow discharge stage

For HiPIMS deposition, it is thought that the loss of the deposition rate is due to the return of ionized sputtered atoms back to the target under the influence of negative target potential. In the DC discharge, the cathode fall thickness  $d_c$  and sheath thickness both reflect how far the electric field can reach in the region between the electrode and plasma; hence, the cathode fall thickness can be calculated through

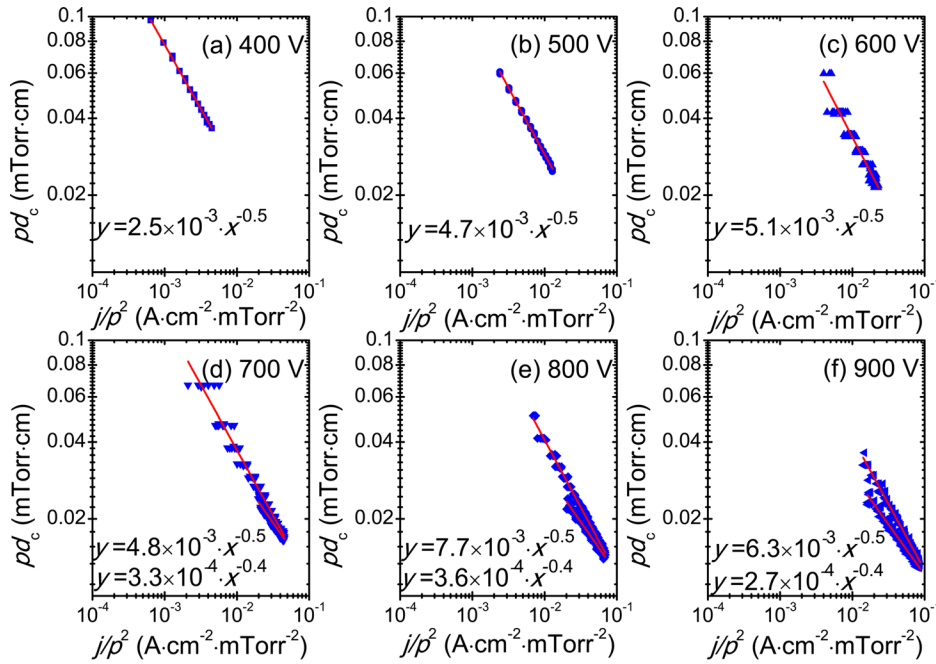


FIG. 6. The variation of  $pd_c$  against  $j/p^2$  at different pulse voltages at 2.5 mTorr.

the Child-Langmuir law in weak collisional sheath theory.<sup>22</sup> Herein, the relationship between reduced cathode fall thickness  $pd_c$  and  $j/p^2$  under different pulse voltage and working pressure conditions is demonstrated in Figs. 6 and 7, respectively. In both conditions, the values of  $pd_c$  decrease as  $j/p^2$  grows.

With the increase of pulse voltage, the current density apparently improves. Meanwhile, the cathode fall thickness reduces. The decrease of  $pd_c$  by increasing the pulse voltage is attributed to the increase in electron kinetic energy. Therefore, the electron-atom ionization cross section increases and the discharge needs less distance to create the negative glow region. However, the  $pd_c$  increases with increased pulse voltage at the same  $j/p^2$  when the pressure is 2.5 mTorr. The strong electric field produced at high voltage can accelerate the ions and results in more efficient sputtering processes. When the pulse voltage is set below 600 V, the cathode fall

thickness monotonically decreases. However, at high pulse voltage it finally increases following the decrease process; hence, the negative glow region at last runs away from the cathode after a moving close process. The increased cathode fall thickness extends the electric field into the ionization region in stage *c*. Therefore, a significant amount of metal ions will be attracted back to the target surface.

In the DC glow discharge process, the relationship between the normalized cathode current density and target voltage under the assumption of linear variation of the electric field over a distance equal to the thickness of the cathode fall is as follows:<sup>18</sup>

$$pd_c = A \cdot (j/p^2)^B, \quad (4)$$

where  $A$  is a variable that depends on the target voltage ( $V_t$ ) and electron emission yield ( $\gamma_i$ ). The curves fitted with

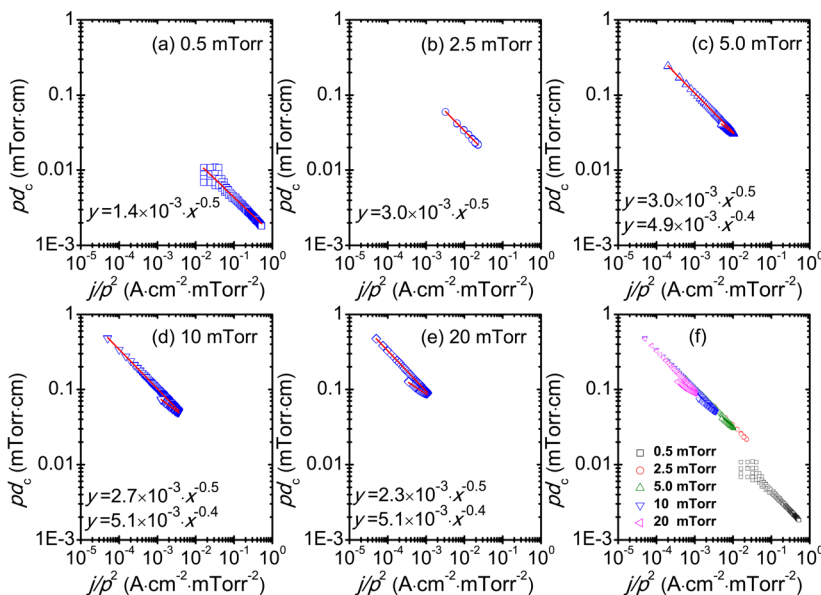


FIG. 7. The variation of  $pd_c$  against  $j/p^2$  at different working pressures at 600 V.

Eq. (4), red lines in the Fig. 7, and the fitting functions are shown in the figures. In stage *b*,  $A$  varied with pulse voltage, and  $B = -0.5$ ; in stage *c*, values of  $A$  are smaller than that in stage *b* and change little, and  $B = -0.4$ . In stage *c*, the scaling relationship between  $pd_c$  and  $j/p^2$  obeys the similarity principle.

The reduced cathode fall thickness  $pd_c$  increased with working pressure. Meanwhile, with a same  $j/p^2$  the value of  $pd_c$  with pressure higher than 2.5 mTorr is the same. Hence, the cathode thickness  $d_c$  at higher pressure is smaller than that at low pressure. Fitting the curves with Eq. (4), as shown in Fig. 6 the scaling relationship between  $pd_c$  and  $j/p^2$  obeys the similarity principle in stages *b* & *c*, respectively. At 0.5 mTorr, the small value of  $A$  can be attributed to low electron yield caused by inefficient electron-atom collision.

#### D. Peak ion densities with the variation of pulse voltage and working pressure

The peak ion density is estimated using the current density at the target as the cathode by using the following equation:<sup>22,23</sup>

$$j = 0.61en_iu_B, \quad (5)$$

where  $e$  is electron charge,  $n_i$  is ion density in the ionization region,  $u_B = \sqrt{k_B T_e / m_i}$  is Bohm velocity of the ions,  $k_B$  is the Boltzmann constant,  $T_e$  is the electron temperature, and  $m_i$  is the argon ion mass.  $T_e$  is selected as 3.5 eV for a typical HiPIMS pulse on process.<sup>2</sup> The gas density is calculated from the ideal gas equation of state, Eq. (6), for a pure Ar gas environment to estimate the plasma ionization degree ( $\alpha$ ).

$$p = Nk_B T, \quad (6)$$

where  $N$  is the Ar gas density and  $T$  is the Ar gas temperature in the chamber (about 300 K). Therefore, the peak ionization degree during each pulse can be calculated through the following equation:

$$\alpha = n_i / N. \quad (7)$$

As shown in Fig. 8(a), both the plasma density and ionization degree monotonically increase with increasing pulse voltages. Two different types of behavior are identified. One for low pulse voltages (400–600 V) where the maximum plasma density is less than  $3 \times 10^{12} \text{ cm}^{-3}$ , and the ionization degree is less than 0.05. It suggests that the HiPIMS discharge under these conditions is similar to DCMS discharge. A different behavior is observed for high pulse voltages (600–950 V), where both the plasma density and the ionization degree are significantly higher. The values of  $1.3 \times 10^{13} \text{ cm}^{-3}$  and 0.16 for the plasma density and ionization degree, respectively, are determined at 950 V. This can be attributed to the transform of normal glow into abnormal glow after 600 V; more secondary electrons can be emitted in the abnormal mode. As the working pressure grows, although the ionization degree decreases, plasma density increases. The ionization energy of the metal atom is much lower than that of Ar atoms; the increase of plasma density can increase the amount of metal atoms. Hence, it is suggested to increase the working pressure appropriately to reach high current and deposition rate.

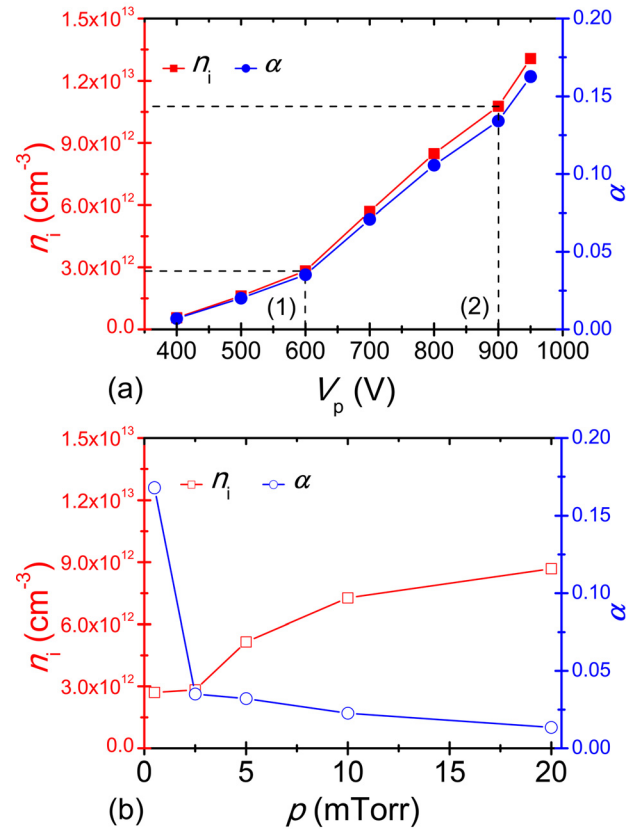


FIG. 8. The ion density and ionization degree with variation of (a) pulse voltages at 2.5 mTorr and (b) working pressures at 600 V.

#### IV. CONCLUSIONS

The temporal evolutions of the target voltage and current waveforms in Cr HiPIMS discharge have been studied as a function of pulse voltage and working pressure. The magnetron sputtering discharge during each pulse sequentially undergoes four main stages. The target voltage - current and voltage-normalized current density characteristics elucidate the change of the discharge mode from gas glow to gas/sputtered material mixed glow as a consequence of high plasma density and gas rarefaction effect. Accompanied by the change in the discharge mode, the sputtering process also steps into self-sputtering. The evolution of the cathode fall thickness was also determined. A noticeable increase of the cathode fall thickness caused by gas rarefaction has been observed at high pulse voltage and working pressure conditions. For a rectangular chromium target plasma density and ionization degree are achieved with HiPIMS with maximum values at  $1.3 \times 10^{13} \text{ cm}^{-3}$  and 0.16, respectively.

#### ACKNOWLEDGMENTS

This research was supported by the project of the National Natural Science Foundation of China (51522106 and 5151101342) and State Key Project of Fundamental Research of China (2013CB632302 and 2017YFB0702300), and Zhejiang Key Research and Development Program (2017C01001).

- <sup>1</sup>J. T. Gudmundsson, N. Brenning, D. Lundin, and U. Helmersson, *J. Vac. Sci. Technol., A* **30**(3), 030801 (2012).
- <sup>2</sup>J. T. Gudmundsson, J. Alami, and U. Helmersson, *Appl. Phys. Lett.* **78**(22), 3427 (2001).
- <sup>3</sup>J. T. Gudmundsson, *Vacuum* **84**(12), 1360–1364 (2010).
- <sup>4</sup>H. Sun, C. K. Wen, S. C. Chen, T. H. Chuang, M. A. P. Yazdi, F. Sanchette, and A. Billard, *J. Alloys Compd.* **688**, 672–678 (2016).
- <sup>5</sup>A. Aijaz, Y. X. Ji, J. Montero, G. A. Niklasson, C. G. Granqvist, and T. Kubart, *Sol. Energy Mater. Sol. Cells* **149**, 137–144 (2016).
- <sup>6</sup>M. Mickan, U. Helmersson, H. Rinnert, J. Ghanbaja, D. Muller, and D. Horwat, *Sol. Energy Mater. Sol. Cells* **157**, 742–749 (2016).
- <sup>7</sup>I. L. Velicu, M. Neagu, and V. Tiron, *J. Supercond. Novel Magn.* **28**(3), 1035–1039 (2015).
- <sup>8</sup>H. Elmkhah, T. F. Zhang, A. Abdollah-Zadeh, K. H. Kim, and F. Mahboubi, *J. Alloys Compd.* **688**, 820–827 (2016).
- <sup>9</sup>D. J. Christie, *J. Vac. Sci. Technol., A* **23**(2), 330–335 (2005).
- <sup>10</sup>J. Vlcek and K. Burcalova, *Plasma Sources Sci. Technol.* **19**(6), 065010 (2010).
- <sup>11</sup>A. Anders, *Surf Coat. Technol.* **205**, S1–S9 (2011).
- <sup>12</sup>J. Alami, K. Sarakinos, G. Mark, and M. Wuttig, *Appl. Phys. Lett.* **89**(15), 154104 (2006).
- <sup>13</sup>A. Anders, J. Andersson, and A. Ehiasarian, *J. Appl. Phys.* **102**(11), 113303 (2007).
- <sup>14</sup>Z. Z. Wu, S. Xiao, Z. Y. Ma, S. H. Cui, S. P. Ji, X. B. Tian, R. K. Y. Fu, P. K. Chu, and F. Pan, *AIP Adv.* **5**(9), 097178 (2015).
- <sup>15</sup>X. P. Qin, P. L. Ke, A. Y. Wang, and K. H. Kim, *Surf Coat. Technol.* **228**, 275–281 (2013).
- <sup>16</sup>C. Q. Huo, M. A. Raadu, D. Lundin, J. T. Gudmundsson, A. Anders, and N. Brenning, *Plasma Sources Sci. Technol.* **21**(4), 045004 (2012).
- <sup>17</sup>G. Y. Yushkov and A. Anders, *IEEE Trans Plasma Sci.* **38**(11), 3028–3034 (2010).
- <sup>18</sup>A. V. Phelps, *Plasma Sources Sci. Technol.* **10**(2), 329 (2001).
- <sup>19</sup>A. E. Wendt, M. A. Lieberman, and H. Meuth, *J. Vac. Sci. Technol., A* **6**(3), 1827–1831 (1988).
- <sup>20</sup>A. E. Wendt and M. A. Lieberman, *J. Vac. Sci. Technol., A* **8**(2), 902–907 (1990).
- <sup>21</sup>Y. Y. Fu, H. Y. Luo, X. B. Zou, and X. X. Wang, *Phys. Plasmas* **22**(2), 023502 (2015).
- <sup>22</sup>M. A. Lieberman and A. J. Lichtenberg, *Principles of Plasma Discharges and Materials Processing*, 2nd ed. (Wiley-Interscience, Hoboken, NJ, 2005).
- <sup>23</sup>K. Yukimura, R. Mieda, K. Azurna, H. Tamagaki, and T. Okimoto, *Nucl. Instrum. Methods, Sect. B* **267**(8–9), 1692–1695 (2009).